Available online at www.sciencedirect.com
ScienceDirect
Catalysis Today 131 (2008) 211–218
CATALYSIS TODAY
www.elsevier.com/locate/cattod

Partial oxidation of methane to synthesis gas over $Co/Ca/Al_2O_3$ catalysts

X.X. Gao, C.J. Huang *, N.W. Zhang, J.H. Li, W.Z. Weng, H.L. Wan *

The State Key Laboratory for Physical Chemistry of Solid Surfaces, Department of Chemistry, Xiamen University, Xiamen 361005, PR China

Available online 26 November 2007

Abstract

A series of calcium-modified alumina-supported cobalt catalysts were prepared with a two-step impregnation method, and the effect of calcium on the catalytic performances of the catalysts for the partial oxidation of methane to syngas (CO and H_2) was investigated at 750 °C. Also, the catalysts were characterized by XRD, TEM, TPR and (*in situ*) Raman. At 6 wt.% of cobalt loading, the unmodified alumina-supported cobalt catalyst showed a very low activity and a rapid deactivation, while the calcium-modified catalyst presented a good performance for this process with the CH_4 conversion of ~88%, CO selectivity of ~94% and undetectable carbon deposition during a long-time running. Characterization results showed that the calcium modification can effectively increase the dispersion and reducibility of Co_3O_4, decrease the Co metal particle size, and suppress the reoxidation of cobalt as well as the phase transformation to form $CoAl_2O_4$ spinel phases under the reaction conditions. These could be related to the excellent catalytic performances of $Co/Ca/Al_2O_3$ catalysts.

Keywords: Partial oxidation of methane; Synthesis gas; Cobalt; Alumina; Calcium modification

1. Introduction

The utilization of nature gas (mainly methane) as a fossil fuel resource and a hydrogen source is attracting more and more attention. Compared with steam and CO_2 reforming of methane, partial oxidation of methane (POM) into syngas is of considerable interest because this reaction is energy saving [1], and the produced syngas has a H_2/CO ratio of 2, which is suitable for use in production of methanol and synthetic fuels [2]. A number of catalysts, including nickel, cobalt and the noble metals (Rh, Pt, Ru, Ir), have been adapted to the partial oxidation of methane [3–12]. Among them, nickel- and cobalt-based catalysts are particularly promising due to their low prices. Much attention has been devoted to nickel catalysts, although the catalysts suffer from deactivation mainly due to carbon deposition and the loss of nickel under high flow rate and high temperature.

Compared to nickel, cobalt has higher melting and vaporizing points. Also, cobalt-based catalysts are less active for syngas methanation. The methanation is especially needed to be considered for the POM process performed in the fluidized bed reactor [13]. Therefore, cobalt-based catalysts may be an interesting alternative to traditional nickel-based catalysts [13,14]. The major drawback with the cobalt catalysts are their lower activities and stabilities [7,8]. Due to low reducibility and the easiness of cobalt metal to oxidize, a higher cobalt loading is often indispensable to the supported cobalt catalyst with high catalytic performance [9,10]. Recently, Co/MgO and Co/Al_2O_3 catalysts have been reported to be active for partial oxidation of methane to syngas [11,12], but their cobalt loadings were as high as 24 wt.%. Since a higher metal loading generally tends to result in more carbon deposition, an efficient cobalt catalyst with lower metal loading is desired.

To improve the catalytic performance of supported nickel and cobalt catalysts for conversion of methane to syngas, the effect of promoter has been widely studied. It has been shown that calcium acts as a good nickel catalyst promoter, improving the coking stability by increasing electron density of the nickel and so decreasing its methane-dehydrogenating power [15–17]. Despite this, few studies have been made on the effect of this promoter on supported cobalt catalyst for the POM reaction.

In this work, partial oxidation of methane to syngas was performed on $Co/Ca/Al_2O_3$ catalysts. The effect of calcium promoter on the catalyst structure and performance was studied by XRD, TEM, TPR and Raman spectroscopy.

* Corresponding authors.
E-mail addresses: huangcj@xmu.edu.cn (C.J. Huang), hlwan@xmu.edu.cn (H.L. Wan).

0920-5861/$ – see front matter © 2007 Elsevier B.V. All rights reserved.
doi:10.1016/j.cattod.2007.10.051

2. Experimental

2.1. Catalyst preparation

Co/Al_2O_3 catalysts were prepared by the wet-impregnation method, using $Co(NO_3)_2{\cdot}6H_2O$ and γ-Al_2O_3 (S_{BET} = 132.6 $m^2\,g^{-1}$) as the metal precursor and the support, respectively. After drying at 110 °C, the resulting material was then calcined in air at 600 °C for 4 h. The calcium-modified alumina-supported cobalt catalysts ($Co/Ca/Al_2O_3$) were prepared with the sequential impregnation. First, the calcium-modified support was prepared by impregnating γ-Al_2O_3 with $Ca(NO_3)_2{\cdot}4H_2O$ aqueous solution, followed by calcining in air at 600 °C for 4 h. Then, the $Co/Ca/Al_2O_3$ catalysts were prepared using the same procedure for the Co/Al_2O_3 catalyst. The prepared catalysts are denoted as xCo/Al_2O_3 and xCo/yCa/Al_2O_3, where x and y refer to the mass percents of Co and Ca, respectively.

2.2. Catalytic reaction

The catalytic reaction was carried out in a fixed-bed vertical quartz reactor (i.d. = 5 mm) under atmospheric pressure. Prior to reaction, the catalyst was reduced at 700 °C in H_2 flow (20 ml/min) for 1 h, followed by Ar purge and heating under Ar flow to the reaction temperature. The reactant gas stream consisted of CH_4, O_2 and Ar with a molar ratio of 2:1:4, controlled by mass flow controllers. After condensing and drying, the reaction effluents were analyzed with an on-line gas chromatography equipped with a TCD and a TDX-01 column.

2.3. Catalyst characterization

X-ray powder diffraction (XRD) measurements were performed on a Rigaku Rotaflex D/max-C X-ray power diffractometer with Cu Kα radiation. The samples were studied either after calcination or after reduction. Average cobalt metal particle size (d) was measured from the XRD line of Co at $2\theta = 44.2°$, using XRD line broadening. Cobalt dispersion (D) was calculated according to the equation [18]: d (nm) = $6.59s/\%D$, where s = 14.6.

Temperature-programmed reduction (TPR) was conducted in a quartz tube of 4 mm diameter with 50 mg sample by raising the temperature from 100 to 900 °C at a rate of 10 °C/min under a 5% H_2/Ar mixture flowing at 30 ml/min. Hydrogen consumption was monitored by a TCD detector after removing the water formed. Before TPR experiments, catalysts were pretreated *in situ* at 500 °C in a flow of moisture-free oxygen for 30 min.

Transmission electron micrographs (TEM) were taken on a TECNAI F-30 FEG electron microscope operating at 300 kV.

Laser Raman spectroscopic (LRS) studies were carried out using Renishaw UV–vis Raman 1000 System equipped with a CCD detector and a Leica DMLM microscope. The line at 514.5 nm of an Ar^+ laser was used for excitation.

Temperature-programmed oxidation (TPO) was performed to measure the amount of carbon deposited on the catalysts. After reaction, the catalysts were cooled down under argon to room temperature, and the TPO experiments were carried out in the same manner as reported in the literature [19].

3. Results and discussion

3.1. Catalytic performance

The effect of calcium content on the catalytic performances of $Co/Ca/Al_2O_3$ catalysts with 6 wt.% Co loading is shown in Fig. 1. The results were obtained after 30 min on stream. As can be seen, the unmodified and the low-calcium content catalysts show very low activities for methane conversion and low selectivities to syngas. Their products are mainly CO_2. With the increase of calcium content, CH_4 conversion and the selectivities to H_2 and CO sharply increase, as opposite to the selectivity to CO_2, and attain their maximum values at calcium content of about 6 wt.%. The CH_4 conversion (89%) and CO selectivity (94%) at that calcium content are around three times higher than those (31% and 28%, respectively) of caiclum-free catalyst, and close to the values predicted by thermodynamic equilibrium [20].

The effect of cobalt loading on the methane conversions of unmodified and calcium-modified Co/Al_2O_3 catalysts is presented in Fig. 2. The unmodified sample keeps a low CH_4 conversion in a wide range of cobalt loading from 3 to 9 wt.%. Not until the loading is increased up to as high as 12 wt.%, is a high activity obtained. At and below 3 wt.% cobalt loading, the calcium-containing sample also shows a low CH_4 conversion. The conversion, however, sharply increases to a maximal value when the cobalt loading is increased from 3 to 6 wt.%, beyond which the conversion remains almost unchanged. This observation clearly shows that much smaller cobalt loading of the calcium-modified catalyst produces a high

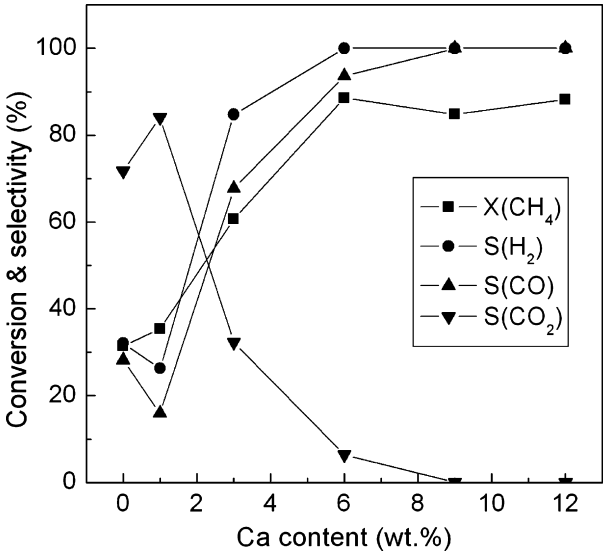

Fig. 1. Effect of Ca content on the catalytic performance of 6Co/xCa/Al_2O_3 catalysts for partial oxidation of methane to syngas. Data were obtained after 30 min on stream. Reaction conditions: T = 750 °C, $CH_4/O_2/Ar$ = 2/1/4, GHSV = 12,000 ml g^{-1} h^{-1}.

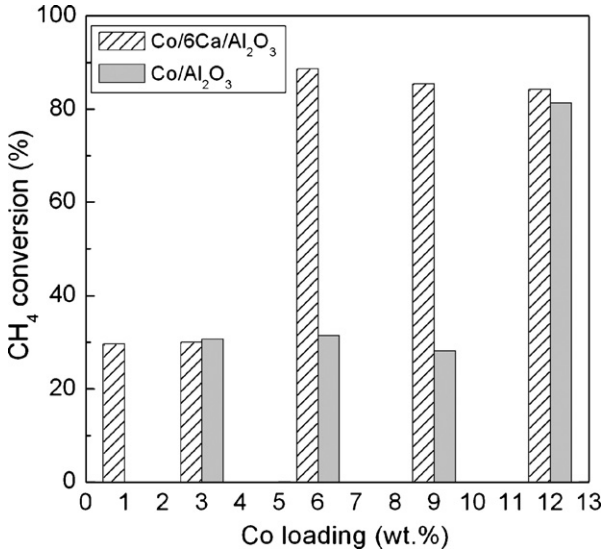

Fig. 2. Effect of cobalt loading on the methane conversion over Co/Al_2O_3 and $Co/6Ca/Al_2O_3$ catalysts. Data were obtained after 30 min on stream. Reaction conditions: $T = 750\ ^\circ C$, $CH_4/O_2/Ar = 2/1/4$, GHSV = 12,000 ml g^{-1} h^{-1}.

catalytic performance for partial oxidation of methane to syngas, as compared to the case of unmodified catalyst.

For $6Co/6Ca/Al_2O_3$ and $6Co/Al_2O_3$ catalysts, the influence of space velocity on the catalytic performance was further studied. As shown in Fig. 3, methane conversion and CO selectivity decrease with the increase in space velocity over $6Co/6Ca/Al_2O_3$ catalyst. The similar results have also been reported for other supported Ni, Co catalysts [21,22]. These results seem to reflect the two-step reaction mechanism that methane total combustion happens first to form CO_2 and H_2O, followed by reforming of methane to syngas [22]. Compared to $6Co/6Ca/Al_2O_3$ catalyst, $6Co/Al_2O_3$ shows much lower activity

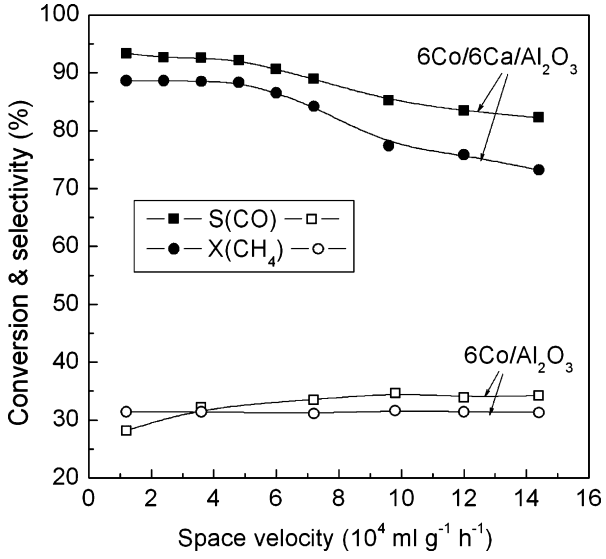

Fig. 3. CH_4 partial oxidation to syngas over $6Co/6Ca/Al_2O_3$ (closed symbols) and $6Co/Al_2O_3$ (open symbols) catalysts as a function of space velocity. Data were obtained after 30 min on stream. Reaction conditions: $T = 750\ ^\circ C$, $CH_4/O_2/Ar = 2/1/4$.

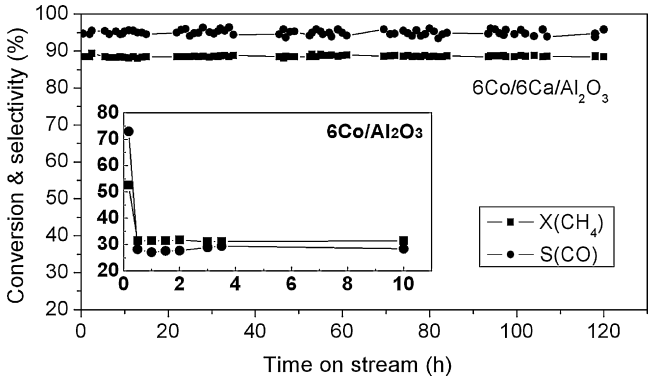

Fig. 4. Alteration of methane conversion and CO selectivity as a function of time on stream over $6Co/6Ca/Al_2O_3$ and $6Co/Al_2O_3$ catalysts. Reaction conditions: $T = 750\ ^\circ C$, $CH_4/O_2/Ar = 2/1/4$, GHSV = 12,000 ml g^{-1} h^{-1}.

and CO selectivity at the whole range of space velocity studied. On this sample, complete oxidation of methane into CO_2 and H_2O is predominant.

Fig. 4 shows the alteration of CH_4 conversion and CO selectivity over $6Co/6Ca/Al_2O_3$ and $6Co/Al_2O_3$ catalysts, as a function of time on stream. During a long time running (120 h), $6Co/6Ca/Al_2O_3$ catalyst gives the CH_4 conversion of ~88% and CO selectivity of ~94% without any loss in catalytic activity and selectivity. After the experiment, it was found that the initially dark catalyst did not change its color. The used sample shows a flat TPO profile (not shown here), implying no carbonaceous deposited or their amounts, which were less than the detection capability of the TPO analysis. On the other hand, $6Co/Al_2O_3$ catalyst shows a low initial activity and a rapid deactivation. The CH_4 conversion and CO selectivity sharply decrease from 53% and 73% to 31% and 28%, respectively, in about 30 min after the feed gas is introduced, and then remain low and unchanged during 10 h on stream. For this catalyst, no coking deposits could be determined by TPO either, but the initially dark catalyst turned light blue, implying that the $CoAl_2O_4$-like compound was probably formed [23].

3.2. Catalyst characterization

The specific surface areas of the catalysts determined by physical adsorption of nitrogen (BET) are shown in Table 1. The surface area is increased firstly by a small amount (1 wt.%) of calcium added, and then decreases continuously with the increase of calcium content, due to the covering and blocking of Al_2O_3 pores by calcium oxide. However, no correlation

Table 1
BET surface area and crystalline phase of the catalysts

Catalyst	Surface area (m^2 g^{-1})	Crystalline phases
$6Co/Al_2O_3$	132.6	Co_3O_4, γ-Al_2O_3
$6Co/1Ca/Al_2O_3$	166.6	Co_3O_4, γ-Al_2O_3
$6Co/3Ca/Al_2O_3$	149.6	Co_3O_4, γ-Al_2O_3
$6Co/6Ca/Al_2O_3$	133.9	Co_3O_4, γ-Al_2O_3
$6Co/9Ca/Al_2O_3$	115.9	Co_3O_4, γ-Al_2O_3
$6Co/12Ca/Al_2O_3$	95.1	Co_3O_4, γ-Al_2O_3

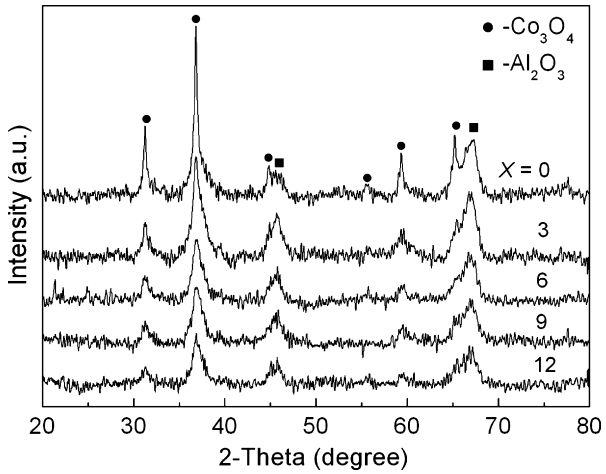

Fig. 5. XRD patterns of $6Co/xCa/Al_2O_3$ catalysts with various calcium contents.

between the surface area and the catalytic activity could be observed.

The XRD results of $6Co/xCa/Al_2O_3$ (x = 0–12 wt.%) catalysts are shown in Fig. 5 and Table 1. No phase containing calcium could be detected for all the calcium-containing samples, indicating that calcium oxide and/or calcium aluminate, which may be produced due to the interaction of calcium with alumina [24], are highly dispersed. In all the samples only γ-Al_2O_3 and Co_3O_4 crystalline phases are observed. The XRD peaks of Co_3O_4 become broader and weaker with the increase of calcium content, indicating an increased dispersion of cobalt oxide species due to calcium addition. Based on the XRD characteristic alone, however, it is difficult to determine the $CoAl_2O_4$ phases for these catalysts, because both Co_3O_4 and $CoAl_2O_4$ have identical XRD patterns [12].

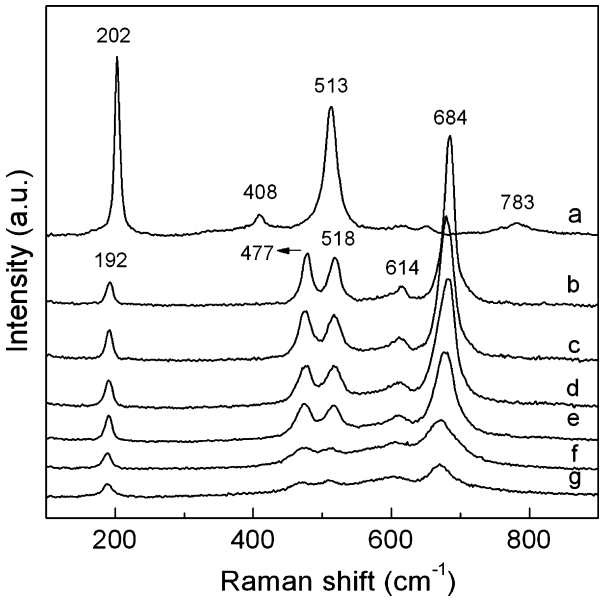

Fig. 6. Raman spectra of (a) $CoAl_2O_4$ prepared by calcining $6Co/Al_2O_3$ at 1200 °C for 4 h, (b) $6Co/Al_2O_3$, (c) $6Co/1Ca/Al_2O_3$, (d) $6Co/3Ca/Al_2O_3$, (e) $6Co/6Ca/Al_2O_3$, (f) $6Co/9Ca/Al_2O_3$ and (g) $6Co/12Ca/Al_2O_3$ samples.

The Raman spectra shown in Fig. 6 give more information on the surface structure of the catalysts. In order to identify the Raman bands of the samples, the Raman spectrum of $CoAl_2O_4$, the reference sample prepared by calcining $6Co/Al_2O_3$ at 1200 °C for 4 h, is also shown in Fig. 6. It is seen that $CoAl_2O_4$ has two strong bands at 202 and 513 cm^{-1} and two weak bands at 408 and 783 cm^{-1}. These bands are absent from the spectra of all the prepared catalysts, indicating that no or little $CoAl_2O_4$ was formed during the preparation. On unmodified and low-calcium content catalysts, a series of strong Raman bands are observed at 684, 614, 518, 477 and 192 cm^{-1}, which are

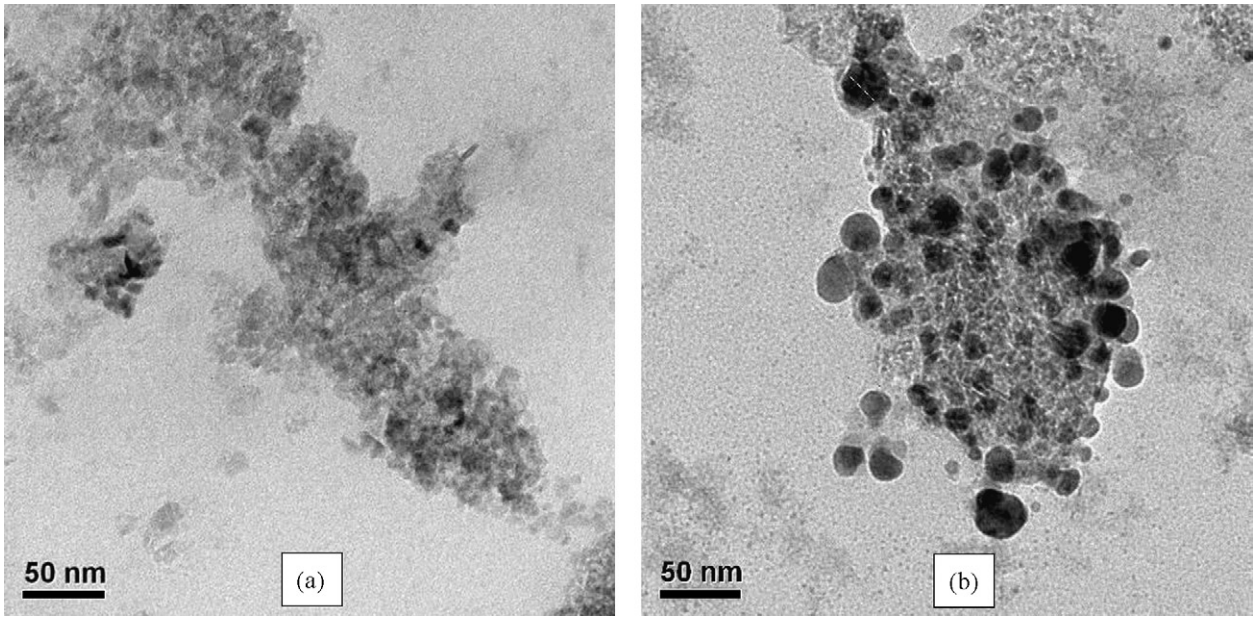

Fig. 7. TEM images of the catalysts: (a) $6Co/6Ca/Al_2O_3$ and (b) $6Co/Al_2O_3$.

assigned to Co_3O_4 spinel [25]. With increasing calcium content, the bands of Co_3O_4 broaden, weaken noticeably and shift to lower wavenumbers, indicating a decrease in particle size [26]. This is in agreement with the XRD results described above, and is also further confirmed by the TEM observations with 6Co/Al_2O_3 and 6Co/6Ca/Al_2O_3 catalysts as shown in Fig. 7. The TEM images demonstrate that on the calcium-modified alumina the cobalt oxide species are well-dispersed, while on the unmodified sample the cobalt oxide species aggregate into large particles.

Fig. 8 shows the TPR profiles of supported cobalt catalysts. For unmodified 6Co/Al_2O_3, two major peaks are found at 565 and 770 °C. The former peak is related to the two-step reduction ($Co_3O_4 \rightarrow CoO \rightarrow Co^0$) of Co_3O_4. The latter, high-temperature peak is assigned to the disordered, X-ray amorphous surface overlayers of Co oxide [23,27], which is assumed to be highly dispersed and interacts strongly with the support. The TPR profiles of calcium-modified catalysts are clearly different from the profiles of the unmodified catalyst. The main pattern with two major peaks is still observed, but the peaks have been shifted. A broad, high-temperature peak at 620–780 °C is observed for all the calcium-containing samples. However, this peak varies with calcium content in a somewhat complicated way. It probably indicates a transformation of the cobalt surface phase caused by the calcium modification. The more significant information is obtained from the peak related to the reduction of Co_3O_4. This peak shifts gradually to a low temperature with the increase of calcium content, indicating that calcium suppresses the interaction of Co_3O_4 with the support and, consequently, brings out an improved reducibility. When the content increases up to 6 wt.%, the peak shifts to lower temperature by as high as around 100 °C. From then on, the peak temperature remains unchanged.

Probably, the hydrophilicity of Ca would also play a role in the TPR procedure. The mass transport of H_2O across the oxide lattice may be influenced by the presence of Ca. Lago et al. reported that in the TPR profiles of $LnCoO_3$ perovskite oxide precursors, the low-temperature peak showed a long tail in the lower temperature and split into two components [28]. Such an observation has been explained as that the reduction is activated and probably controlled by mass transport of H_2 or/and H_2O across the lattice. As seen in Fig. 8, however, for the low-temperature peak in the TPR profiles of Co/Ca/Al_2O_3 catalysts, neither the long tail nor the split can be observed. This indicates that the mass transport of H_2O influenced by Ca is less notable. Thus, it can be assumed that the hydrophilicity of Ca is not a main factor affecting the TPR results in this work.

In order to study the relationship between reducibility and catalytic performance of the catalysts, the variation of the reduction peak ascribed to Co_3O_4 with calcium content is plotted in Fig. 9, accompanied by that of methane conversion for comparison. The catalytic data are taken from Fig. 1. With calcium content increasing, the methane conversion and the peak temperature vary in opposite directions, attain the maximum and minimum values, respectively, at the same calcium content (6 wt.%). Beyond that content, both remain unchanged. This observation clearly indicates that the catalytic activity is closely related to the reducibility of the supported Co_3O_4. It is more likely that an increased reducibility of the calcium-modified catalysts is a main factor, which is responsible for their higher catalytic performances for partial oxidation of methane to syngas. This is consistent with a previous report [29] that cobalt-based catalysts are active for POM to syngas only when promoted with elements, which favored Co reducibility.

XRD measurements were performed in an attempt to examine the cobalt particle sizes of the catalysts after reduction at 700 °C. These data are summarized in Table 2. The calcium-modified catalysts show smaller crystallites by XRD than do unmodified catalysts with the same cobalt loading. In the cobalt loading range of 6–12 wt.%, the calcium-containing sample has cobalt dispersion approximately two times higher than the

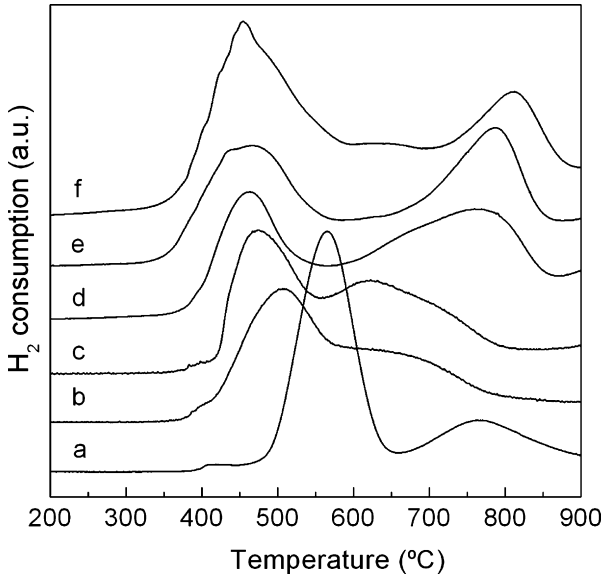

Fig. 8. TPR profiles of the catalysts: (a) 6Co/Al_2O_3; (b) 6Co/1Ca/Al_2O_3; (c) 6Co/3Ca/Al_2O_3; (d) 6Co/6Ca/Al_2O_3; (e) 6Co/9Ca/Al_2O_3; (f) 6Co/12Ca/Al_2O_3.

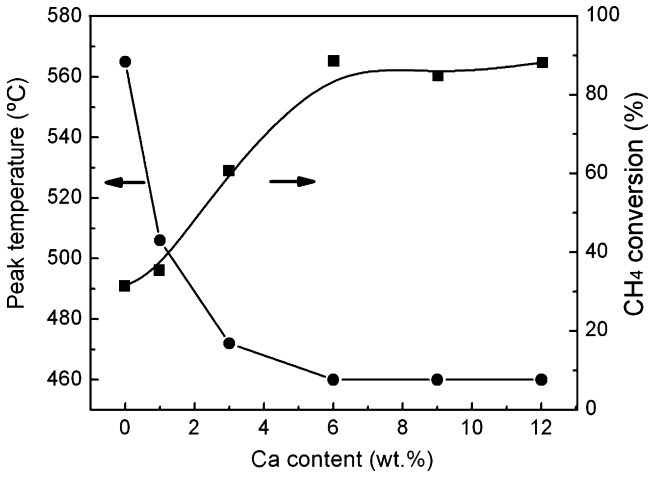

Fig. 9. variations of peak temperature of Co_3O_4 reduction and methane conversion as function of calcium content in the 6Co/xCa/Al_2O_3 catalysts. The peak temperatures and the CH_4 conversions are taken from Figs. 8 and 1, respectively.

Table 2
Average cobalt particle sizes of unmodified and 6% Ca-modified Co/Al_2O_3 catalysts[a]

Co loading (wt.%)	Particle size (nm)		Size ratio of unmodified/modified	Dispersion (%)	
	Unmodified	Modified		Unmodified	Modified
6	15.1	8.3	1.8	6.4	11.6
9	18.9	9.1	2.1	5.1	10.6
12	22.3	12.6	1.8	4.3	7.6

[a] The catalysts were reduced in H_2 at 700 °C for 1 h. The particle sizes were measured by X-ray diffraction line broadening. The dispersion were calculated according to the equation: d (nm) = 6.59s/%D [18].

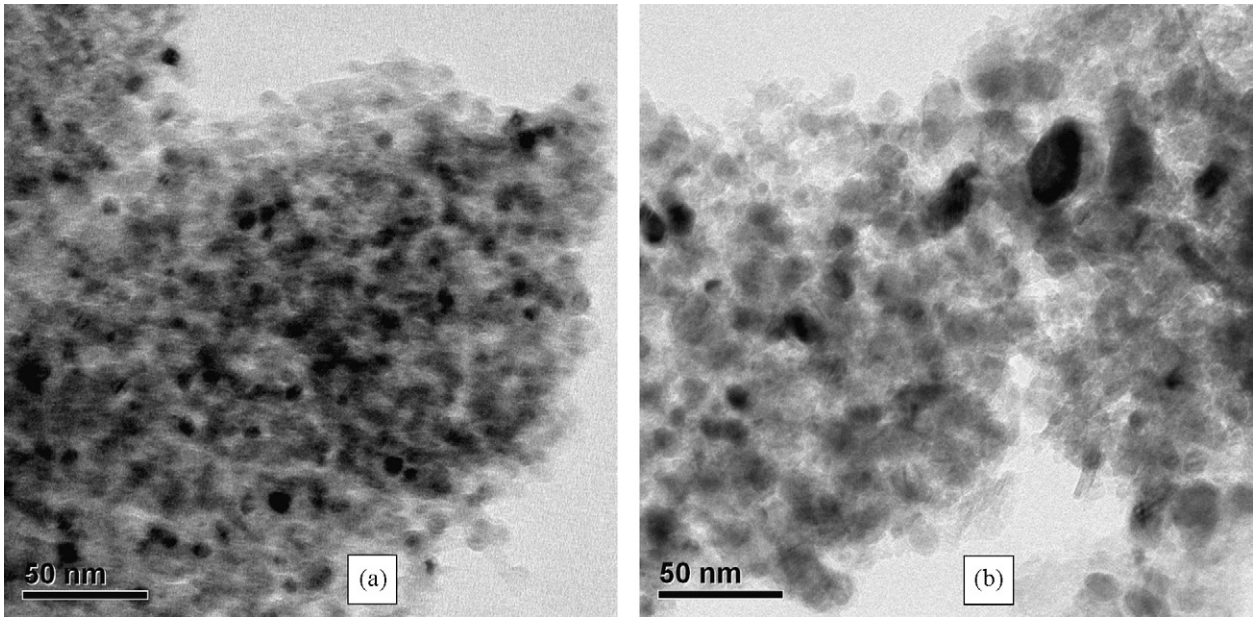

Fig. 10. TEM images of the catalysts after reduction in H_2 at 700 °C for 1 h. (a) $6Co/6Ca/Al_2O_3$ and (b) $6Co/Al_2O_3$.

identical calcium-free sample. The TEM images shown in Fig. 10 are also consistent with the above results. Finely dispersed cobalt particles on $6Co/6Ca/Al_2O_3$ and partially aggregated large particles on $6Co/Al_2O_3$ are observed. The former case clearly indicates a high dispersion of cobalt particles. These results are in agreement with the studies on Ni/Al_2O_3 and $Ni/CaO–Al_2O_3$ catalysts [30]. It has been shown that the particle size of metallic nickel was decreased by CaO modification. To some extent, the highly dispersed metal crystallites are responsible for a higher catalytic activity. Also, they are expected to be more resistant to carbon deposition, as claimed by many authors [30–32].

Fig. 11 shows the Raman spectra of $6Co/Al_2O_3$ and $6Co/6Ca/Al_2O_3$ catalysts after on-stream process at 750 °C for 10 and 120 h, respectively. The bands due to Co_3O_4 at 190, 472, 514, 606 and 673 cm^{-1} are observed for $6Co/6Ca/Al_2O_3$. The presence of Co_3O_4 over this sample could be attributed, at least in part, to the oxidation occurred under the ambient conditions. After reaction, the reactor was cooled down in argon atmosphere and the catalysts were exposed to air at room temperature to obtain Raman spectra. Although the laser power was reduced to ~1.5 mW to avoid sample damage due to the laser irradiation, it is not possible to completely avoid oxidation of the surface metallic cobalt by air. However, this cannot explain the Raman spectrum of $6Co/Al_2O_3$ catalyst after reaction. In the spectrum, the bands assigned to $CoAl_2O_4$ are clearly observed at 202, 410, 515 and 783 cm^{-1}, indicating that during the reaction, the metallic cobalt over the sample is oxidized and transformed into $CoAl_2O_4$. With calcium

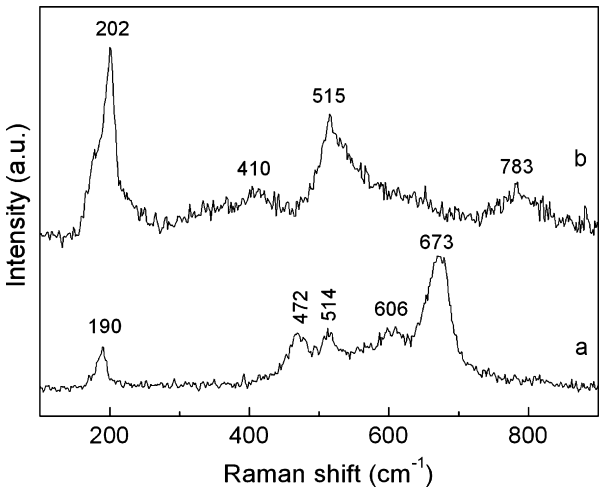

Fig. 11. Raman spectra of (a) $6Co/6Ca/Al_2O_3$ and (b) $6Co/Al_2O_3$ catalysts after reaction for 120 and 10 h, respectively, under the same conditions as noted in Fig. 4.

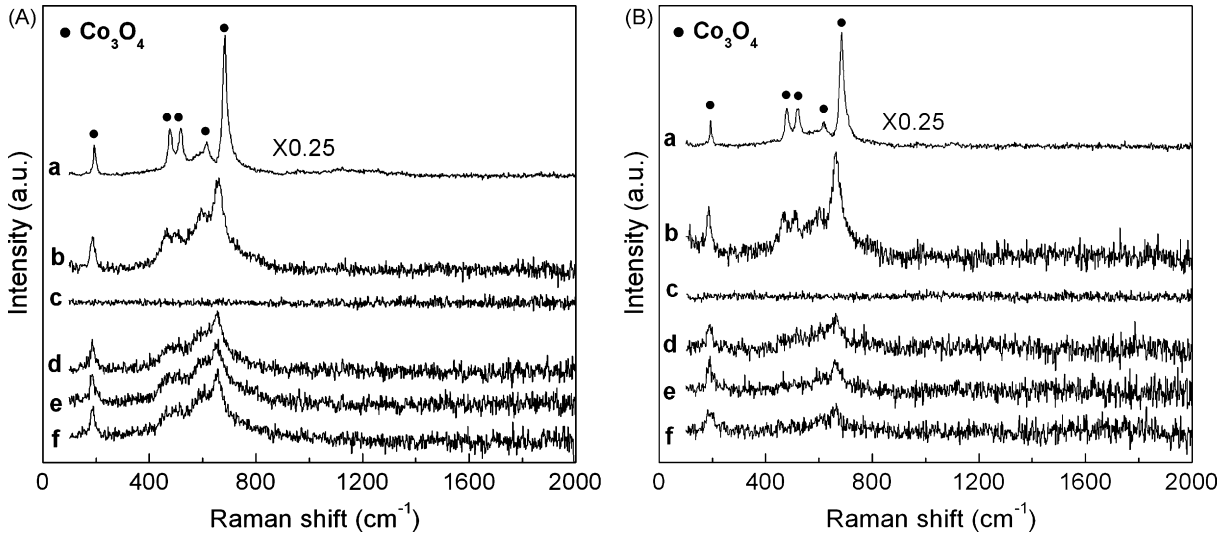

Fig. 12. *In situ* Raman spectra of (A) $6Co/Al_2O_3$ and (B) $6Co/6Ca/Al_2O_3$ catalysts recorded at (a) room temperature and after (b) heating to 700 °C in O_2/Ar, (c) Ar purge followed by reduction in H_2/Ar flow for 30 min and (d–f) reaction in CH_4/O_2/Ar flow (CH_4/O_2/Ar = 2/1/4) for 10, 20 and 30 min.

modification, such a phase transformation is suppressed, as a result of a decrease in the interaction between cobalt and alumina. Similar results have been reported for Ca-modified Al_2O_3-supported Ni catalysts [31]. It was revealed that the $CaAl_2O_4$ compounds existed between Ni and Al_2O_3 could effectively suppress the formation of $NiAl_2O_4$ during POM to syngas reaction.

To explore the catalyst structure under the POM reaction conditions, the *in situ* Raman spectroscopy was performed for $6Co/Al_2O_3$ and $6Co/6Ca/Al_2O_3$ catalysts. The results are shown in Fig. 12. When the temperature is increased to 700 °C in O_2/Ar flow, on both the samples the bands assigned to Co_3O_4 weaken, broaden and shift to lower temperatures due to the temperature effect. After reduction in H_2 flow for 30 min, these bands vanish completely, indicating a transformation of Co_3O_4 into metallic cobalt. On exposure to the reaction atmosphere (CH_4/O_2/Ar flow), both the reduced catalysts recover their Co_3O_4 bands to some extent. This recovery, however, is much less pronounced for the calcium-modified catalyst. On that sample the Raman bands keep very low intensities during 30 min on stream, which is quite different from the case of the unmodified sample. This observation demonstrates that, compared to Al_2O_3-supported cobalt, Ca/Al_2O_3-supported cobalt is less susceptive to reoxidation under the POM reaction conditions. It could account for the great difference in catalytic stability between the two catalysts. In the *in situ* Raman spectra obtained in the atmosphere of POM reaction, no bands related to carbon species are observed for both $6Co/Al_2O_3$ and $6Co/6Ca/Al_2O_3$ catalysts, indicating that coking, which often leads to the deactivation of non-noble catalysts for POM reaction, is negligible in the present work. This is also in agreement with the TPO results as mentioned above.

4. Conclusions

The results of this study demonstrate that $Co/Ca/Al_2O_3$ catalyst is more active and stable for partial oxidation of methane to syngas compared to Co/Al_2O_3 catalyst. The Ca-modified catalyst has high activity, selectivity and stability, even at a low cobalt loading (6 wt.%). On the other hand, the unmodified catalyst with the same cobalt loading shows a low initial activity and a rapid deactivation due to the transformation of cobalt metal into $CoAl_2O_4$. In $Co/Ca/Al_2O_3$ catalysts, the presence of calcium effectively increases the dispersion and reducibility of Co_3O_4, decreases the Co metal particle size, and suppresses the reoxidation of metallic cobalt as well as the phase transformation to form $CoAl_2O_4$ spinel phases under the reaction conditions. These can be related to the excellent catalytic performance of $Co/Ca/Al_2O_3$ catalysts.

Acknowledgements

This project is supported by the Ministry of Science and Technology of China (2005CB221401, 2005CB221408), the National Natural Science Foundation of China (20433030, 20021002 and 20423002) and Key Scientific Project of Fujian Province, China (2005HZ01-3).

References

[1] N. Nichio, M. Casella, O. Ferretti, M. Gonzalez, C. Nicot, B. Moraweck, R. Frety, Catal. Lett. 42 (1996) 65–72.
[2] R.S. Drago, K. Jurczyk, N. Kob, A. Bhattacharyya, J. Masin, Catal. Lett. 51 (1998) 177–181.
[3] A.T. Ashcroft, A.K. Cheetham, J.S. Foord, M.L.H. Green, C.P. Grey, A.J. Murrell, P.D.F. Vernon, Nature 344 (1990) 319–321.
[4] D. Dissanayake, M.P. Rosynek, K.C.C. Kharas, J.H. Lunsford, J. Catal. 132 (1991) 117–127.
[5] T. Hayakawa, A.G. Andersen, M. Shimizu, K. Suzuki, K. Takehira, Catal. Lett. 22 (1993) 307–317.
[6] P.M. Torniainen, X. Chu, L.D. Schmidt, J. Catal. 146 (1994) 1–10.
[7] V.R. Choudhary, A.M. Rajput, B. Prabhakar, A.S. Mamman, Fuel 77 (1998) 1803–1807.
[8] A. Slagtern, U. Olsbye, Appl. Catal. A: Gen. 110 (1994) 99–108.
[9] V.R. Choudhary, S.D. Sansare, A.S. Mamman, Appl. Catal. 90 (1992) L1–L5.

[10] Y.F. Chang, H. Heinemann, Catal. Lett. 21 (1993) 215–224.
[11] H.Y. Wang, E. Ruckenstein, J. Catal. 199 (2001) 309–317.
[12] H.Y. Wang, E. Ruckenstein, Catal. Lett. 75 (2001) 13–18.
[13] Å. Slagtern, H.M. Swaan, U. Olsbye, I.M. Dahl, C. Mirodatos, Catal. Today 46 (1998) 107–115.
[14] A.P.E. York, T. Xiao, M.L.H. Green, Top. Catal. 22 (2003) 345–358.
[15] T. Horiuchi, K. Sakuma, T. Fukui, Y. Kubo, T. Osaki, T. Mori, Appl. Catal. A 144 (1996) 111–120.
[16] J.R. Rostrup-Nielsen, Catal. Today 37 (1997) 225–232.
[17] O. Yamazaki, T. Nozaki, K. Omata, K. Fujimoto, Chem. Lett. 21 (1992) 1953–1954.
[18] R.C. Reuel, C.H. Bartholomew, J. Catal. 85 (1984) 63–77.
[19] M.C.J. Bradford, M.A. Vannice, Appl. Catal. A 142 (1996) 73–96.
[20] M.A. Pena, J.P. Gomez, J.L.G. Fierro, Appl. Catal. A 144 (1996) 7–57.
[21] S. Yang, J.N. Kondo, K. Hayashi, M. Hirano, K. Domen, H. Hosono, Appl. Catal. A 277 (2004) 239–246.
[22] K. Nakagawa, N. Ikenaga, Y. Teng, T. Kobayashi, T. Suzuki, Appl. Catal. A 180 (1999) 183–193.
[23] P. Arnoldy, J.A. Moulijn, J. Catal. 93 (1985) 38–54.
[24] T. Horiuchi, H. Hidaka, T. Fukui, Y. Kubo, M. Horio, K. Suzuki, T. Mori, Appl. Catal. A 167 (1998) 195–202.
[25] T.C. Xiao, S.F. Ji, H.T. Wang, K.S. Coleman, M.L.H. Green, J. Mol. Catal. A 175 (2001) 111–123.
[26] M.A. Vuurman, D.J. Stufkens, A. Oskam, G. Deo, I.E. Wachs, J. Chem. Soc., Faraday Trans. 92 (1996) 3259–3265.
[27] H.C. Tung, C.T. Yeh, C.T. Hong, J. Catal. 122 (1990) 211–216.
[28] R. Lago, G. Bini, M.A. Peña, J.L.G. Fierro, J. Catal. 167 (1997) 198–209.
[29] H.M. Swaan, R. Rouanet, P. Widyananda, C. Mirodatos, Stud. Surf. Sci. Catal. 107 (1997) 447–453.
[30] L.Y. Fu, W.G. Xie, S.J. Lu, F.L. Qiu, Sci. China, Ser. B 43 (2000) 154–161.
[31] Y. Lu, Y. Liu, S.K. Shen, J. Catal. 177 (1998) 386–388.
[32] Z. Xu, Y.M. Li, J.Y. Zhang, L. Chang, R.Q. Zhou, Z.T. Duan, Appl. Catal. A 210 (2001) 45–53.